International Journal of Multiphase Flow 35 (2009) 533–549

Contents lists available at ScienceDirect

International Journal of Multiphase Flow

journal homepage: www.elsevier.com/locate/ijmulflow

Modeling of binary droplet collisions for application to inter-impingement sprays

Sayop Kim [a], Doo Jin Lee [a], Chang Sik Lee [b,*]

[a] Graduate School of Hanyang University, 17 Haengdang-dong, Seongdong-gu, Seoul 133-791, Republic of Korea
[b] Department of Mechanical Engineering, Hanyang University, 17 Haengdang-dong, Seongdong-gu, Seoul 133-791, Republic of Korea

ARTICLE INFO

Article history:
Received 10 October 2008
Received in revised form 18 February 2009
Accepted 18 February 2009
Available online 26 February 2009

Keywords:
Droplet collision
Collision model
Collision outcomes
Inter-impingement spray
KIVA-3V code

ABSTRACT

In this paper, we focused on modeling the collision phenomenon between two liquid droplets for application in spray simulations. It has been known that the existing O'Rourke collision model widely used in CFD codes is inaccurate in determining collision outcomes and droplet behavior. In addition, since the collision probability of the model follows a statistical approach involving computational cell geometry, the prediction results should be strongly dependent on the cell size. As a result, to more accurately calculate droplet collisions, the technique for predicting the droplet velocity and its direction after collision must be extended for use in spray modeling. Further, it is also necessary to consider all the possible collision outcomes, such as bouncing, stretching separation, reflexive separation and coalescence. Therefore, this paper describes the appropriateness of a composite concept for modeling collision outcomes and the implementation of deterministic collision algorithms into a multidimensional CFD code for the calculation of post-collisional droplet movements. Furthermore, the existing model does not consider the formation of satellite droplets. For this reason, our present modeling concept includes a fragmenting droplet collision model. Using the present model, we have validated the collision interactions between liquid droplets under high Weber number conditions by comparing our calculations with experimental results from a binary droplet collision. This paper also deals with the application of the model to inter-impingement sprays by analyzing the atomization characteristics, such as mean droplet size and velocity, spray tip penetrations and spray-shapes of the impinging spray using the suggested collision algorithms and then comparing the results with available experimental data.

1. Introduction

In the case of a dense and high Weber number spray region, the atomization characteristics are the result of the competition between the droplet breakup and the binary droplet collision processes. Droplet breakup is mainly induced by interactions between spray droplets and gas motion, which is called aerodynamic breakup, and droplet collision is a mutual impact caused by differences in the velocity and direction of the droplets. In particular, multiple injections or mutual impingement sprays cause repetitive collision events, resulting in breakups that form several satellite droplets or a combination of droplet masses. Then the droplet number, size, velocity and spatial distribution pattern are significantly altered according to the various collision outcomes, bounce, coalescence and separating processes. Therefore, the collision dynamics of liquid droplets has been of interest in various spraying processes.

Numerous experimental studies have focused on the basic mechanisms of binary droplet collision. The researchers have divided the possible collision outcomes into bouncing, coalescence, reflexive separation and stretching separation. A bouncing collision is when a gas film prevents contact between the droplet surfaces, causing the droplets to bounce apart. Coalescence refers to a collision in which two droplets permanently combine. This tends to happen under low Weber number conditions. A separation collision occurs when two droplets impact and then separate into two or more droplets. According to the detailed mechanism of the separation, a separation collision can be divided further into two types, a stretching separation or reflexive separation. Using this classification system, Ashgriz and Poo (1990) have described the detailed collision phenomena and their characteristics.

Another major objective of droplet collision studies has been determining the parameters and their respective values that define the criterion for differentiating between collision types. Many experimental investigations (see e.g. Ashgriz and Poo, 1990; Estrade et al., 1999; Orme, 1997; Qian and Law, 1997) have proven that, regardless of the liquid type, the distinct outcomes of binary droplet collisions can be delineated on a Weber number-Impact parameter plot. Brazier-Smith et al. (1972) used the energy balance equation to determine whether the collision event would be a coalescence or stretching separation. Ashgriz and Poo (1990) also derived a theoretical prediction for reflexive

* Corresponding author. Tel.: +82 2 2220 0427; fax: +82 2 2281 5286.
E-mail address: cslee@hanyang.ac.kr (C.S. Lee).

0301-9322/$ - see front matter © 2009 Elsevier Ltd. All rights reserved.
doi:10.1016/j.ijmultiphaseflow.2009.02.010

and stretching separation based on the energy balance theory and showed reliable experimental results that supported their theory. Furthermore, Estrade et al. (1999) conducted experiments to derive a theoretical equation for a boundary curve to predict bouncing.

Recently, the developments in droplet collision algorithms have been of interest in the field of spray modeling. In general, two possible methods for collision algorithms in CFD code exist such as the statistical and the deterministic approach. In views of statistical approach, Sommerfeld (2001) developed the stochastic inter-particle collision model that relies on the generation of fictitious collision partner and the calculation of the collision probability according to kinetic theory. The O'Rourke's collision model (O'Rourke, 1981) is another one of the models which follow the statistical approach. This concept does not require the exact location of the two colliding droplets and the probability of collision is computed statistically based on the local distribution of the droplet presence. The O'Rourke's model has been currently used for most of the Lagrangian spray simulations adopting the stochastic parcel method (Reitz and Diwakar, 1987) in numerous CFD code because it does not need high computational cost. On the other hand, O'Rourke's collision model has some problems with predicting collision outcomes because it only considers two main outcomes: coalescence and stretching separation. Further, in this model, even if stretching separation occurs, the sizes of the two colliding droplets do not change, and satellite droplets do not form. From this reason, Aumann et al. (2002) and Ko et al. (2003) reported that the O'Rourke's model tends to over-predict the mean droplet size and they proposed a composite model for predicting all collision outcomes. Furthermore, Ashgriz and Poo (1990), Qian and Law (1997) and Brenn et al. (2001) have reported that several satellite droplets are created during the separation processes. In regards to this phenomenon, the models for fragmenting collision, which consider the formation of satellite droplets, were recently developed by Georjon and Reitz (1999), Ko and Ryou (2005) and Munnannur and Reitz (2007).

One important feature of O'Rourke's model is the assumption that collision occurs only if the two parcels belong to the same computational cell and the probability of collision is determined by a statistical approach. On the other hand, Nordin (2000) reported that this method is limited by its grid dependency, as well as by the location of the collisions, because the cells of the gas phase are used to calculate the collision probability. To remedy these problems, he suggested a methodology for a mesh-independent collision, which introduces simple formulations where the determination of the collision probability is based on the proximity of the two colliding parcels, not on the cell size.

In the present modeling concept, to ensure that the spray simulation is adequate for all outcomes, all the possible collision outcomes were regarded and implemented into the KIVA code (see Amsden, 1997) using the criteria derived from preceding studies (see e.g. Ashgriz and Poo, 1990; Brazier-Smith et al., 1972; Estrade et al., 1999). The collision probability was resolved according to the deterministic approach of Nordin's concept (2000). The present study focuses on the physics of the post-collision movement of liquid droplets, which includes the velocities and directions of droplets after collision, because other collision models do not consider the detailed physics of droplet behavior in three-dimensional space. Therefore, this study uses vector analysis to derive the formula for the behavior of the interacting droplets and satellite droplets. Then, using the present model based on these concepts, the predicted results are validated and compared to available experimental results for binary droplet collisions. Moreover, the present model was applied to predict the internal structure of the inter-impingement spray, and these results were also compared to those from previous experiments.

2. Droplet collision theories and modeling

2.1. Determination of important parameters

In general, the three important dimensionless parameters that characterize the collision phenomenon include the Weber number (We), droplet diameter ratio (Δ) and impact parameter (B), which are, respectively, defined by

$$We = \frac{\rho_f d_2 u_{12}^2}{\sigma_f} \tag{1}$$

$$\Delta = \frac{r_2}{r_1} \tag{2}$$

$$\text{and } B = \frac{X}{r_1 + r_2} \tag{3}$$

where the subscripts 1 and 2 indicate the larger and smaller droplet, respectively. Here, the impact parameter X is defined as the projection of the distance between the droplet centers in the direction normal to that of the relative velocity, $\vec{u}_{12}$ as shown in Fig. 1. So the quantity B becomes the dimensionless impact parameter that varies from 0 to 1. In the case of a head-on collision, B is zero and the relative velocity vector coincides with the center-to-center line. On the other hand, if $B \geqslant 0$, the collision is off-axis. The impact parameter is derived by $X = b\sin|\beta - \gamma|$.

Another important parameter is the relative velocity between the two droplets. If the two droplets travel forming a collision angle, α, the magnitude of relative velocity is determined as

$$|\vec{u}_{12}| = \sqrt{|\vec{u}_1|^2 + |\vec{u}_2|^2 - 2|\vec{u}_1||\vec{u}_2|\cos\alpha} \tag{4}$$

2.2. Mechanisms of droplet collision

Generally speaking, the possible outcomes of a binary droplet collision can be divided into four different types: bouncing, coalescence, reflexive separation and stretching separation. Fig. 2 shows schematic diagrams of the different collision outcomes.

As the two droplets approach each other under certain conditions of relative velocity and impact parameter, a gas layer may prevent direct contact between the droplet surfaces, causing the droplets to bounce apart, similar to the impact between rigid spheres. Therefore, a bouncing collision is dependent on the ambient gas characteristics, such as density of the surrounding gas, and the flow field surrounding the droplets (see e.g. Ashgriz and Poo, 1990). On the other hand, if the droplets travel slowly enough, then the air may exit before the droplets contact each other, and the droplets may combine and become a single droplet. This type of collision is referred to as coalescence. In the mean time, Orme (1997) classified the coalescence into two types, permanent

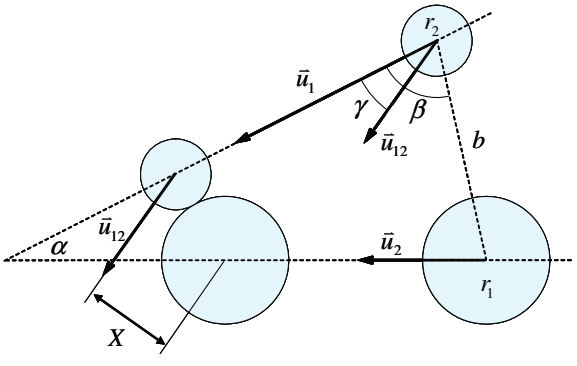

Fig. 1. Schematic of the binary droplet collision.

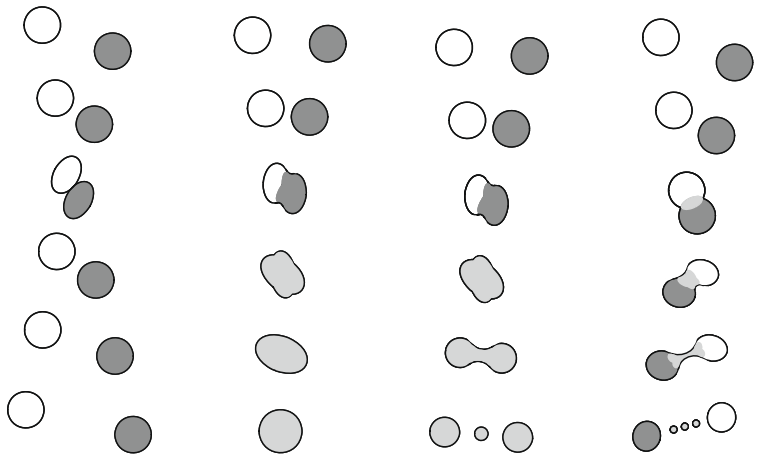

Fig. 2. Mechanisms of droplet collision.

coalescence and temporary coalescence followed by disruption. However, we regarded the coalescence only as the permanent coalescence and classified the temporary coalescence into the stretching separation or the reflexive separation according to pattern of disruption.

A separation collision occurs when the two droplets combine temporarily and then separate into two or more droplets. The separation collision can be further sub-classified into two types according to the physics of the separation process. A reflexive separation occurs when two droplets collide nearly head-on. In this case, the masses of the two droplets temporarily coalesce and form a cylinder that has rounded ends, and the cylinder ultimately breaks up. In contrast, a stretching separation occurs with large impact parameter collisions. When the collision occurs in the off-axis, only a portion of each droplet contacts the other one and the droplets interact. The remaining portions of the droplets do not interact and they will continue to flow in their own directions, thus stretching the interaction region.

2.3. Model formulations

This study focuses mainly on the implementation of a collision model in CFD codes. In general, there are two possible ways to implement the droplet collision algorithms: a statistical approach or a deterministic approach. First of all, with the statistical approach, the possibility of a collision for a pair of parcels is statistically determined. O'Rourke (1981) adopted the statistical approach for droplet collision modeling. In contrast, with the deterministic approach, the exact positions and velocity vectors for a pair of parcels are used to determine the collision possibility. In this study, using the Nordin's concept (2000) and modeling the post-collision characteristics, the deterministic approach was implemented in the KIVA code. In order to consider the satellite droplet formation, the Munnannur's fragmenting collision model (2007) was used. And the present model also considered all possible collision outcomes. Table 1 provides the details of our collision model adaptation.

Furthermore, in order to consider the liquid dispersion caused by aerodynamic force, the WAVE-RT model (see Beale and Reitz, 1999) was used to describe the liquid jet dispersion and the breakup of droplet separated from the liquid jet. In the current computation, a method of stochastic parcel representing each liquid droplet was used and tracked in a Lagrangian manner (see Dukowicz, 1980).

2.3.1. O'Rourke's collision model – statistical approach

The most popular collision model used in CFD codes today is O'Rourke's collision model (1981). The model follows the statistical approach in predicting the collision events. The concept of the statistical collision modeling is based on the creation of a fictitious collision partner, which is done with the help of local size and velocity distributions of the droplet phase (Sommerfeld, 2001; Blei et al., 2002). This model only regards collisions of parcels that lie in the same computational cell. Then, assuming that both parcels are homogeneously distributed inside the cell volume, V_{cell}, the collision frequency of a larger droplet against all the smaller droplets is given by

$$\nu_{12} = \frac{N_2}{V_{cell}} \frac{\pi}{4} (d_1 + d_2)^2 |\vec{u}_{12}| \tag{5}$$

According to the Poisson distribution concept, the probability of no collision is determined as $P_0 = \exp(-\nu_{12} \Delta t)$ (O'Rourke and Bracco, 1980). Next, a random number ξ is sampled from a uniform distribution between 0 and 1. Then, if $\xi > P_0$, a collision between the two parcels is assumed to take place, and if not so, no collision occurs. In terms of the collision frequency, the probability of a droplet collision is affected by the cell volume.

In this model, only two main collision outcomes are usually regarded following the transition condition introduced by the Brazier-Smith et al. (1972). The critical impact parameter that divides coalescence and stretching separation is shown in Fig. 3 and the value of the critical impact parameter is chosen as the square root of the coalescence efficiency, which is estimated as:

$$e_{coal} = \min(1.0, 4.8 f(\gamma)/\mathrm{We}) \tag{6}$$

where $f(\gamma) = \gamma^3 - 2.4\gamma^2 + \gamma$ and $\gamma = 1/\Delta$. Following the statistical approach, if a random number between 0 and 1 is larger than the critical number, the collision outcome is assumed to be a stretching separation, otherwise it is considered to be coalescence.

With regards to post-collision characteristics, O'Rourke (1981) derived the equation for the post-collision velocities of the droplets. If the two droplets permanently coalescence, the velocity of the combined droplets is calculated as:

$$\vec{u}_{new} = \frac{m_1 \vec{u}_1 + m_2 \vec{u}_2}{m_1 + m_2} \tag{7}$$

If stretching separation occurs, both droplets are reformed again and their size is assumed to stay constant even though the interacting droplets experience a mass change in reality. In addition, there is no consideration for the formation of satellite droplets.

Table 1
Specification of the collision models.

		O'Rourke's model	Present model
Collision condition		Statistically determined	Nordin (2000)
Satellite droplet formation		–	Munnannur and Reitz (2007)
Post-collision characteristics		–	Currently suggested
Collision regimes	Bounce	–	Estrade et al. (1999)
	Coalescence	Brazier-Smith et al. (1972)	Brazier-Smith et al. (1972)
	Stretching separation	Brazier-Smith et al. (1972)	Brazier-Smith et al. (1972)
	Reflexive separation	–	Ashgriz and Poo (1990)

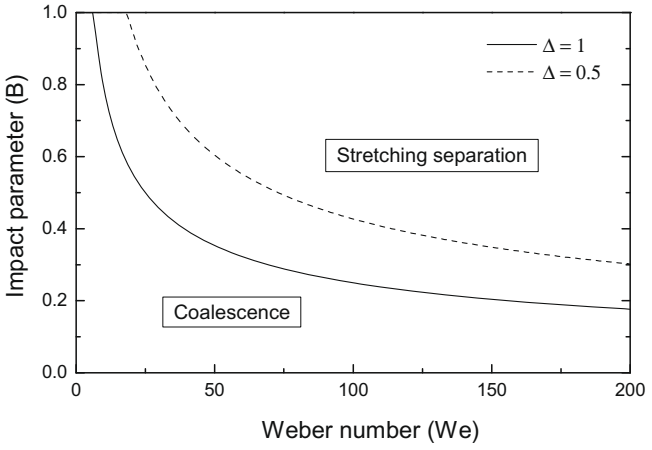

Fig. 3. Influence of droplet size ratio on the coalescence–stretching separation criterion (Brazier-Smith et al., 1972).

The velocities of the interacting droplets can be treated by energy and momentum conservation and derived as:

$$\vec{u}_{new,i} = \frac{r_i^3\vec{u}_i + r_j^3\vec{u}_j + r_j^3(\vec{u}_i - \vec{u}_j)z}{r_i^3 + r_j^3} \quad (i,j = 1,2) \tag{8}$$

Here, z indicates the fraction of energy that is dissipated during collision and is determined by

$$z = \left(\frac{B - \sqrt{e_{coal}}}{1 - \sqrt{e_{coal}}}\right) \tag{9}$$

2.3.2. Fragmenting droplet collision model

Munnannur and Reitz (2007) developed a predictive collision model that focuses particularly on the fragmentation in stretching separation and reflexive separation under high Weber number conditions ($We > 40$). They modeled the fragmentation and the formation of satellite droplets under the assumption that the interacting droplets form an elongating ligament that breaks up into smaller droplets as shown in Fig. 4.

(1) Stretching separation: For the stretching separation, Munnannur and Reitz (2007) proposed a separation volume coefficient (C_{VS}) to determine the temporal evolution of a ligament that is composed of parts of the interacting volumes of the two colliding droplets.

$$C_{VS} = \frac{E_{strtch} - E_{surten} - E_{dissip}}{E_{strtch} + E_{surten} + E_{dissip}} \tag{10}$$

where E_{strtch} is the total effective stretching kinetic energy and E_{surten} is the surface energy in the region of interaction derived by Ashgriz and Poo (1990). E_{dissip} is the viscous dissipation and is assumed to be 30% of the total initial kinetic energy of the droplets. To estimate C_{VS}, the E_{strtch} and E_{surten} are calculated by

$$E_{strtch} = \frac{1}{2}\rho_f|\vec{u}_{12}|^2\left(\frac{1}{6}\pi d_1^3\right)\left(\frac{\Delta^3}{(1+\Delta^3)^2}\right)\left[(1+\Delta^3) - (1-B^2)(\varphi_2 + \Delta^3\varphi_1)\right] \tag{11}$$

$$E_{surten} = \sigma_f\left[2\pi\left(\frac{1}{6}\pi d_1^3\right)d_1\tau(\Delta^3\varphi_2 + \varphi_1)\right]^{1/2} \tag{12}$$

If $C_{VS} < 0$, it is assumed that fragmentation does not occur. Ashgriz and Poo (1990) derived the fraction of the volume lost from the smaller and the larger droplets to form the ligament by

$$\psi_i = C_{VS}\varphi_i \quad (i = 1,2) \tag{13}$$

where,

$$\varphi_1 = \begin{cases} 1 - \dfrac{(2-\tau)^2(1+\tau)}{4}, & h > r_1 \\ \dfrac{\tau^2(3-\tau)}{4}, & h \leqslant r_1 \end{cases} \tag{14}$$

$$\varphi_2 = \begin{cases} 1 - \dfrac{(2\Delta-\tau)^2(\Delta+\tau)}{4\Delta^3}, & h > r_2 \\ \dfrac{\tau^2(3\Delta-\tau)}{4\Delta^3}, & h \leqslant r_2 \end{cases} \tag{15}$$

and $h = (r_1 + r_2)(1 - B)$, $\tau = (1 - B)(1 + \Delta)$. With the fraction of the separated volume, the elongating ligament from the interacting volume can be determined. In this model, the initial shape of the mass that connects the end-droplets is assumed to be a uniform cylinder of length equal to its radius, so the initial radius of the ligament can be calculated by

$$r_0 = \left[\frac{4}{3}(\psi_1 r_1^3 + \psi_2 r_2^3)\right]^{1/3} \tag{16}$$

Assuming that the ligament radius at the breakup is r_{bu}, the non-dimensional ligament radius at breakup $\bar{r}_{bu} = r_{bu}/r_0$ can be calculated by solving

$$\frac{0.75}{\sqrt{2}}(k_1 k_2)We_0^{1/2}\bar{r}_{bu}^{7/2} + \bar{r}_{bu}^2 - 1 = 0 \tag{17}$$

The solution was numerically calculated using the linear interpolation method. Then, assuming the ligament breakup is dominated by Rayleigh-type instability, the radius of the satellite droplets formed from the ligament breakup can be determined by

$$r_{sat} = 1.89 r_{bu} \tag{18}$$

Here, the model constants k_1 and k_2 are assumed to be 8.5 and 0.45, respectively, based on the literature of Munnannur and Reitz (2007). But, in this study, the value of k_1 is suggested to be 11.5 to give an agreeable comparison with the current experimental results, which will be explained in the next section.

In this model, an important time scale is suggested and details of the fragmentation modeling in the stretching separation will be explained in terms of the time scale. The time scale T is determined by

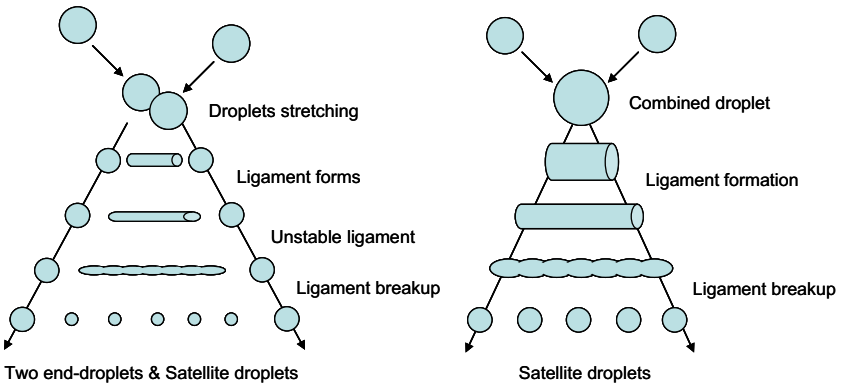

(a) Stretching separation (b) Reflexive separation

Fig. 4. Schematic of ligament formation and breakup.

$$T = 0.75k_2\sqrt{We_0} \tag{19}$$

where $We_0 = \rho_f(2r_0)|\vec{u}_{12}|^2/\sigma_f$. In the case of stretching separation of Munnannur's model, if $C_{VS} \geqslant 0$ and $T \leqslant 2$, the ligament is assumed to contract into a single satellite with a radius equal to the initial radius of the ligament, r_0. If $C_{VS} \geqslant 0$ and $T > 2$, the ligament is assumed to be stretched and its break up is governed by Eq. (17), and the number of satellite droplets is calculated from the mass conservation of the ligament assuming satellites of uniform size by

$$N_{sat} = \frac{3}{4}\left(\frac{r_0}{r_{sat}}\right)^3 \tag{20}$$

Since the current experimental result is well matched with the original criteria, Munnannur's assumption for stretching separation is used in the current calculation without modification.

(2) Reflexive separation: For the reflexive separation, it is assumed that two droplets temporarily combine and form a cylindrical ligament where the ligament volume is equal to the sum of the volumes of the interacting droplets. Therefore, the initial radius of the ligament becomes

$$r_0 = (r_1^3 + r_2^3)^{1/3} \tag{21}$$

As with stretching separation, the size of the satellite droplets is calculated using Eqs. (17) and (18). In the study of Munnannur and Reitz (2007), the fragmentation in reflexive separation was modeled using the time scale, T. They assumed that, if $T \leqslant 3$, only a single satellite droplet is formed, otherwise, the ligament is assumed to stretch and break up. Here, the ligament is supposed to disintegrate into droplets of uniform size, with two droplets as the end-droplets and the rest as satellites. Therefore, it is assumed that satellite droplets are always formed in this model. However, according to the experimental studies (see e.g. Ashgriz and Poo, 1990; Qian and Law, 1997), there can be a reflexive separation with no satellite droplet, especially under a low Weber number condition. In particular, following the experiments of droplet collision by Ashgriz and Poo (1990), a one-satellite reflexive separation case did not result in a uniform droplet size for the end-droplets and a single satellite, that is, the satellite is usually smaller than the end-droplets.

From this reason, the criteria were modified in the current study. Considering the ligament breaks up into two end-droplets and satellites in the reflexive separation, the number of satellite droplets is determined by

$$N_{sat} = \frac{3}{4}\left(\frac{r_0}{r_{sat}}\right)^3 - 2 \tag{22}$$

If $N_{sat} \leqslant 0$, it is assumed that the ligament breaks up with no satellite droplet and the two end-droplets have their own radius. If $0 < N_{sat} < 1$, the ligament cannot disintegrate into more than two droplets that have a radius r_{sat}. So, in this case, it is assumed that a single satellite droplet is formed that is smaller than the two end-droplets. On the other hand, if $N_{sat} > 1$, the ligament should break up into uniform droplets, such that the two end-droplets and the satellite droplets have an identical radius, r_{sat}.

2.3.3. Deterministic approach to collision modeling

With the existing collision model (see O'Rourke, 1981), the probability of collision and the impact parameter are statistically determined, resulting in less-detailed collision characteristics related to post-collision velocities and moving directions. In the current study, the impact parameter and the collision direction are calculated in a deterministic manner. Above all, the present concept uses Nordin's mesh independent collision condition (see Nordin, 2000) for determining whether two parcels collide effectively. He suggested that collision between two parcels occurs if their trajectories intersect and the intersection point is reached within an integration time step at the same time. However this condition is computationally expensive when applying to all the parcels in the computation. So, we can sort out pairs of parcels that could never contact each by incorporating two requirements in the concept. The first requirement is that the two parcels are traveling towards each other, which is fulfilled if the following condition is satisfied:

$$|\vec{u}_{12}| = (\vec{u}_2 - \vec{u}_1)\cdot\frac{(\vec{p}_2 - \vec{p}_1)}{|\vec{p}_2 - \vec{p}_1|} < 0 \tag{23}$$

Here, $\vec{u}_i$ and $\vec{p}_i$ are the velocity vector and the position vector of the colliding droplets. The second requirement is that the parcels' relative displacements within a computational time step must be larger than the distance between them and this is represented by:

$$|\vec{u}_{12}|\Delta t > |\vec{p}_2 - \vec{p}_1| - (r_1 + r_2) \tag{24}$$

So, in order to determine the probability of a collision, three-dimensional vector components for velocity and position must be provided, and the vector analysis is used to define the impact parameter. The impact parameter is calculated by measuring the exact positions of the parcels.

As introduced in preceding section, in the existing CFD codes, the droplet velocity after collision is calculated without consideration for the colliding direction, so that all the components of the droplet velocity in multidimensional coordinates are treated by Eq. (8).

However, the effective velocity change in stretching and reflexive separations necessarily happens in the direction of the relative velocity. In addition, the velocity of the satellite droplets must be calculated with a consideration for the colliding direction. Therefore, the present study proposes a method to correct the velocity change along the relative velocity vector in cases of stretching separation and reflexive separation. In the same way, for a bouncing regime, it is necessary to consider the line of impact, which is the common normal to the surface of contact during the impact. The determination of velocity change is detailed in the Appendix.

2.3.4. Transition boundary for collision regimes

Earlier studies on droplet collision have focused on the various regimes for collision outcomes between two liquid droplets, and these studies have provided parameters and their values to characterize the boundaries for different types of collisions. Some generalized collision outcomes have been reported based on a number of experimental studies and these outcomes can be categorized into four distinct types, namely bouncing, coalescence, stretching separation and reflexive separation. It has been shown that these collision regimes can be delineated on a Weber number-Impact parameter. Using the criteria for these collision regimes, the current study accounts for all the possible collision outcomes.

The critical impact parameter, which divides into the coalescence and the stretching separation, was derived by Brazier-Smith et al. (1972). They assumed that the rotational energy of the combined mass of two colliding droplets should be less than the surface energy required to reform the coalesced droplet. The value of the critical impact parameter is chosen as the square root of the coalescence efficiency as estimated by Eq. (6). Here, if $B > \sqrt{e_{coal}}$, the collision outcome is assumed to be a stretching separation, and if not so, it is treated as a coalescence.

Another critical Weber number-impact parameter plot that demarcates regions of the coalescence and the reflexive separation is based on the theory of Ashgriz and Poo (1990). According to their study, if the effective reflexive kinetic energy is more than 75% of the nominal surface energy of the combined spherical mass, reflexive separation is assumed to occur. The criteria under which a reflexive separation will occur is determined by:

$$We > \frac{3[7(1+\Delta^3)^{2/3} - 4(1+\Delta^2)]\Delta(1+\Delta^3)^2}{(\Delta^6\eta_1 + \eta_2)} \tag{25}$$

where $\eta_1 = 2(1-\xi)^2(1-\xi^2)^{1/2} - 1$, $\eta_2 = 2(\Delta-\xi)^2(\Delta^2-\xi^2)^{1/2} - \Delta^3$, and $\xi = 0.5B(1+\Delta)$.

In order to find the boundary of bouncing, Estrade et al. (1999) showed the theoretical prediction of bouncing and compared it to experimental measurements. Boundary criterion for droplet bouncing is derived by assuming that the initial kinetic energy of the droplet does not exceed the energy required to produce a limit deformation. If the condition of Eq. (26) is satisfied, the colliding droplets are assumed to bounce off each other:

$$We \geqslant \frac{\Delta(1+\Delta^2)(4\phi' - 12)}{\chi_1\{\cos[\sin^{-1}(B)]\}^2} \tag{26}$$

where ϕ' is a shape factor of value 3.351 and χ_1 is defined by the following equations,

$$\chi_1 = \begin{cases} 1 - 0.25(2-\tau)^2(1+\tau) & \text{for } \omega > r_1 \\ 0.25\tau^2(3-\tau) & \text{for } \omega \leqslant r_1 \end{cases} \tag{27}$$

with $\tau = (1-B)(1+\Delta)$, and $\omega = (r_1 + r_2)(1-B)$.

2.3.5. Droplet breakup model – WAVE-RT model

In a real injection system, liquid jet is injected and dispersed as numerous droplets. This is referred to as the primary breakup. Then, the separated droplets experience a breakup due to the aerodynamic force, and this is called the secondary breakup. The hybrid breakup model concept is a combination of the primary breakup model and the secondary breakup model as depicted in Fig. 5. Many researchers have proven that the hybrid breakup models give a good accuracy of prediction. Moreover according to application of the secondary breakup models, there have been proposed several hybrid models, i.e. WAVE-RT, WAVE-TAB, WAVE-DDB and so on. Park et al. (2003) showed the comparison of the prediction accuracy of the models, and reported that the WAVE-RT model give a relatively good results for the spray simulations. From this reason, in this study, the WAVE-RT model (Beale and Reitz, 1999) was used as the droplet breakup model.

The WAVE model (see Reitz, 1987) is based on a primary order linear analysis of a Kelvin–Helmholtz instability growing on the surface of a liquid jet penetrating into an incompressible gas. Under this concept, it is assumed that the jet surface is covered with a sinusoidal wave, and then a part of the unstable liquid surface is separated from the liquid jet into droplets. With this model, the primary breakup is modeled by postulating that the new droplets are formed from a parent parcel representing the liquid jet, and then a new stochastic parcel for separated droplets is applied to the computation. In the literature of Reitz, 1987, he resolved the general dispersion equation and showed the solution of maximum growth rate Ω_{KH} and corresponding wavelength Λ_{KH} as:

$$\frac{\Lambda_{KH}}{r} = 9.02\frac{(1+0.45Z^{1/2})(1+0.4T^{0.7})}{(1+0.87We_g^{1.67})^{0.6}} \tag{28}$$

$$\Omega_{KH}\left[\frac{\rho_f r^3}{\sigma}\right]^{1/2} = \frac{(0.34+0.38We_g^{1.5})}{(1+Z)(1+1.4T^{0.6})} \tag{29}$$

where $Z = \sqrt{We_f}/\mathrm{Re}_f$, $T = Z\sqrt{We_g}$, $\mathrm{Re}_f = \rho_f u_d r/\mu_f$, $We_f = \rho_f u_d^2 r/\sigma_f$, and $We_g = \rho_g u_d^2 r/\sigma_f$. Then critical droplet radius r_c separated from the liquid jet and breakup time can be calculated by substituting above solution to the following equations.

$$r_c = B_0\Lambda_{KH} \tag{30}$$

$$\tau_{KH} = \frac{3.726B_1 r}{\Omega_{KH}\Lambda_{KH}} \tag{31}$$

Here, the empirical constants are recommended to be set according to the test conditions. The optimized value for the constants were selected in order to match the calculated spray tip penetration with the measurement, and set to as $B_0 = 4.5$, and $B_1 = 40$.

The Rayleigh–Taylor (RT) model (see Su et al., 1996) is based on the wave instability theory. In this model, it is assumed that the

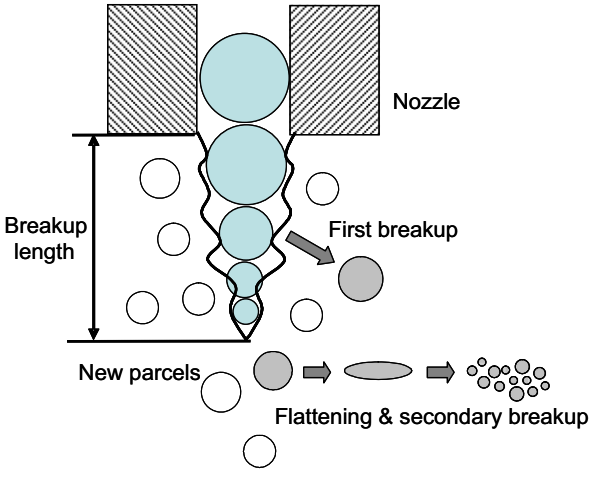

Fig. 5. Schematic of hybrid breakup model.

disintegration of the droplet is induced by the instability of the surface between two fluids, as in the case of the acceleration normal to the interface. In the model, the fastest growing RT wave Ω_{RT}, the corresponding wavelength Λ_{RT}, and wave number K_{RT}, are determined as:

$$\Omega_{RT} = \sqrt{\frac{2}{3\sqrt{3\sigma_f}} \frac{[-(\vec{g}+\vec{a})(\rho_f-\rho_g)]^{1.5}}{\rho_f+\rho_g}} \tag{32}$$

$$\Lambda_{RT} = 2\pi C_{RT}/K_{RT} \tag{33}$$

$$K_{RT} = \sqrt{\frac{-(\vec{g}+\vec{a})(\rho_f-\rho_g)}{3\sigma_f}} \tag{34}$$

where $\vec{g}$ and $\vec{a}$ are the acceleration in the direction of the gravity and drag force, respectively. In this calculation, the empirical constant C_{RT} was selected as 1.5. The RT model assumes if the wavelength is smaller than the droplet diameter, the RT wave begins to grow. Then the wave growth time is tracked and if the time elapses over the breakup time τ_{RT}, the droplet is assumed to break up to smaller droplet which diameter is r_c.

$$\tau_{RT} = C_\tau/\Omega_{RT} \tag{35}$$

$$r_c = \pi C_{RT}/K_{RT} \tag{36}$$

Here, the empirical constants C_τ and C_{RT} were set to as 8 and 1.5, respectively.

3. Experimental and computational conditions

3.1. Experiment for binary droplet collision

In this study, the experiment for equal-sized droplet collision was conducted to validate the droplet collision models. The experimental setup is shown in Fig. 6. The experimental apparatus consists of the droplet generators equipped with VOAG (Vibrating Orifice Aerosol Generator) and a high-speed visualization system. The droplet generator is operated on the basis of the Rayleigh theory (see Rayleigh, 1878) for the instability and breakup of a cylindrical liquid jet. This equipment includes an orifice disk through which the liquid jet passes. By applying the optimal frequency generated by a function generator onto the orifice disk, the issuing liquid jet becomes destabilized and disintegrates into uniform liquid droplets.

In this experiment, two droplet generators were equipped with a two-dimensional traverse system and two streams of liquid droplets were injected downward with a certain collision angle. The test liquid was purified water, and its important physical properties, i.e. density, surface tension, and viscosity are 998 kg/m^3, 0.073 kg/s^2 and 0.001 kg/ms, respectively. The orifice disk, which had a diameter of 90 μm, was used for both the two droplet generators, so the droplet diameter ratio (Δ) becomes unity. The injection velocity of liquid jet is approximately 9.5 m/s, and the measured droplet diameter is 175 μm. The relative velocity between the colliding droplets is determined by controlling the collision angle according to Eq. (4). Furthermore, in order to record the detailed collision processes, a high-speed camera was used and the measurements were then made on the recorded frames with a frame rate of 20,000 fps.

Even though the current study adopted the purified water as a test liquid for the binary droplet collision experiments, the information obtained from the water-droplet can be applied to the other liquid types by introducing the dimensionless parameters, such as Weber number, droplet diameter ratio and impact parameter. It is based on the previous report of Ashgriz and Poo, 1990. In addition, previous experiments (see Estrade et al., 1999 and Chen, 2007) have shown that any liquid types have a similar pattern of collision outcome distribution in terms of these parameters. From this reason, in this study, the validated collision models from the water-droplet collision experiment were used to simulate the inter-impingement sprays of light-oil.

3.2. Calculation condition for inter-impingement spray

Maruyama et al. (2001) and Chiba et al. (2000) experimentally investigated the inter-impingement process in the diesel spray system. They discussed the effect of the impingement angle and the impingement distance on spray tip penetration, tip velocity and spray volume. In this system, two sprays are mutually injected and impinged so that numerous droplets collide frequently and the spatial distribution of the spray can be controlled according to the impingement condition. In the present work, in order to validate the droplet collision models, inter-impingement sprays were simulated using the KIVA-3V code.

The three-dimensional computational domain for the current calculation was made using the KIVA mesh generator with the cell size set as 2 mm in three axes. The 2000 parcels were assumed to be injected for respective sprays during a whole calculation time of 2.9 ms, so total number of parcels was 4000. Then the WAVE model and the present collision model create a number of new parcels for

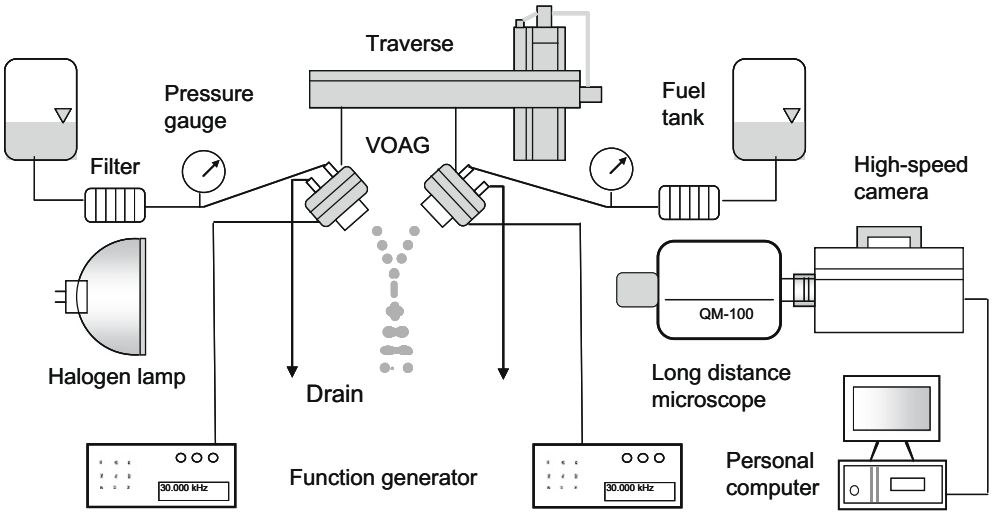

Fig. 6. Schematic diagram of experimental apparatus for binary droplet collision.

satellite droplet formation, such that the total number of parcels is dependent on the conditions of the injection and the impingement.

The calculation test conditions were adopted from the experimental conditions of Maruyama et al. (2001). In their experiment, light oil was injected from two single-hole nozzles into a vessel. The surrounding gas was pressurized at 1.0 MPa, and the room temperature was kept constant. The diameter of the nozzle hole was 0.25 mm and the injection pressure was set to 19.6 MPa. They tested one impingement angle (θ) and four impingement distances (S_z). According to the impingement distance, they divided into the spray-to-spray and jet-to-jet impingements on the basis of the break-up length, which was 36 mm in their experiment. In the present work, we tested two of these conditions: spray-to-spray impingement (S_z=50 mm) and impingement near the break-up length (S_z=33 mm) with a fixed impingement angle, $\theta = 90°$.

In order to specify the behavior of the impingement spray, the spray tip penetration was defined as the sum of the distance from the nozzle tip to the impingement point, S_z and the distance from the impingement point to the spray tip, S_t as shown in Fig. 7. In addition, to investigate the atomization characteristics, such as the mean droplet size and velocity, the measuring points were arranged at intervals of 5 mm as illustrated in Fig. 7. In the experiment of Maruyama et al. (2001), they set one measuring point on the tip of spray shape at 2 ms after the start of injection.

4. Results and discussion

The present study attempts to validate the currently suggested droplet collision model and then applies the model to inter-impingement sprays. First, the calculation is compared to the binary droplet collision experiment performed in the present study, then the collision models are validated in order to be applied to the inter-impingement sprays. Second, in order to test the present model and the O'Rourke's collision model, the inter-impingement experiments of Maruyama et al. (2001) and Chiba et al. (2000) were reviewed. Finally, we investigated the calculated and measured atomization characteristics.

4.1. Validation of binary droplet collision

Fig. 8 shows a collision regime map produced by the current experiment for equally sized water droplet collisions under atmospheric conditions. As mentioned previously, four different types of collision outcomes are clearly delineated by Weber number-Impact parameter plots, i.e. L1, L2, and L3 that are calculated using the formulations from Brazier-Smith et al. (1972), Ashgriz and Poo (1990) and Estrade et al. (1999). Therefore, it is appropriate to implement the curves in the CFD code for boundaries between regimes in order to predict all the possible collision outcomes: bounce, coalescence, stretching separation and reflexive separation.

The present model predictions were validated by comparing with experimental results for satellite droplet formation. Fig. 9 shows the predicted and measured satellite droplet number from binary droplet collisions between equally sized water droplets specifically for stretching separation and reflexive separation collisions. The scattered numbers indicate the measured number of satellite droplets obtained in the current experiment. Using currently modified criteria to predict the satellite droplet number, this comparison shows good qualitative agreement in general. In particular, contrary to the assumption that a satellite droplet is always formed in the reflexive separation with the original Munnannur's criterion, the reflexive separation with no satellite droplet is well predicted up to Weber number of 47.

In this study, the collision between two parcels was calculated using the deterministic approach of Nordin's mesh independent collision concept (see Nordin, 2000). The formation of satellite droplets was considered using the Munnannur's fragmenting collision model (see Munnannur and Reitz, 2007). In addition, post-collision characteristics, such as droplet velocity and moving direction, were newly modeled by a deterministic approach in the present model. Finally the results of the simulation were compared with current experimental data on colliding streams from two water droplets as shown in Fig. 10. The comparisons are presented for each of the four different collision outcomes: coalescence, bounce, reflexive separation and stretching separation. In Fig. 10, the present model demonstrates the resemblance to realistic droplet streams. The important thing is that the present model with Munnannur's model can predict the formation of satellite droplets and their moving direction. Here, the model assumption has one parcel representing all of the satellites, even if two or more satellite droplets are created, as for example, in the stretching separation of Fig. 10(d).

However, in the case of O'Rourke's model, the probability of a collision is statistically calculated based on the cell volume in Eq. (5). In the current test, width and height of the computational

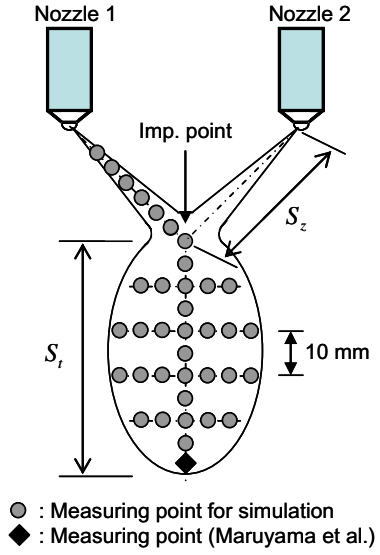

Fig. 7. Schematic diagram of inter-impingement spray.

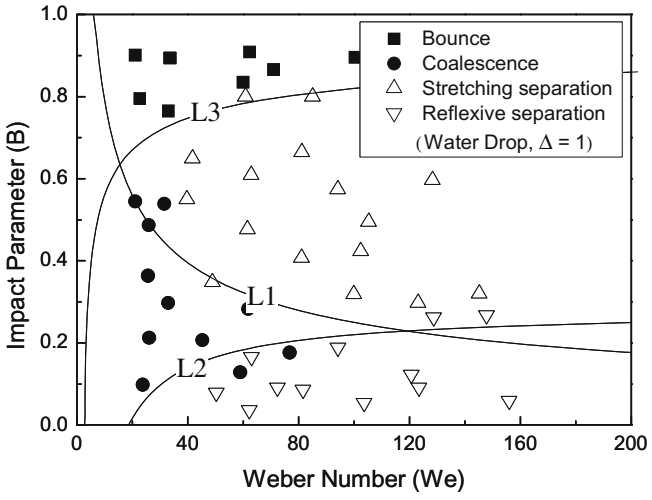

Fig. 8. Collision regime map.

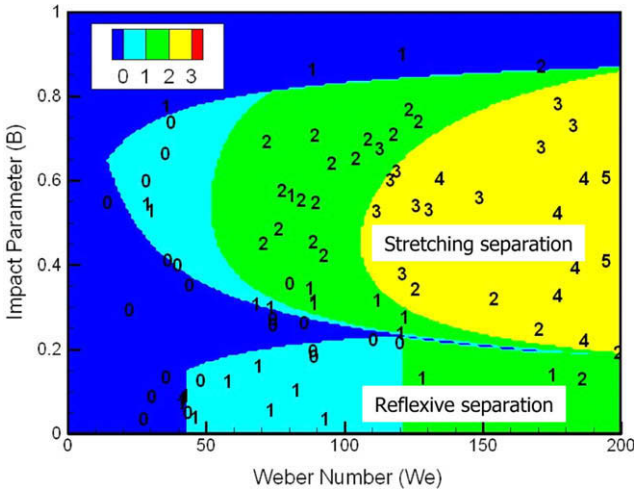

Fig. 9. Number of satellite droplets.

mesh are 2 mm and two parcels are injected in the same cell as illustrated in Fig. 10(a). According to the statistical approach discussed in Section 2.3.1, only the parts from all the parcels that lie in the same cell happen to collide, even if they are in close proximity. Moreover, since the impact parameter that classifies a collision outcome is randomly determined, coalesced droplets are intermittently shown regardless of their exact position. Furthermore, it is assumed that the stretching separated droplets only change their velocity, but do not change their size or result in satellites. Therefore, the droplets located outside the stream result in a stretching separation collision as shown in Fig. 10(c).

4.2. Test for grid sensitivity

This section describes the grid sensitivity of the collision models. Especially, to test the patterns of grid dependency, three impact points (IP) were put on a middle section of a hexagonal cell as shown in Fig. 11. Here, the IP ① is a cell-centered point, and the IP ② and ③ are located on the cell surface and the cell vertex,

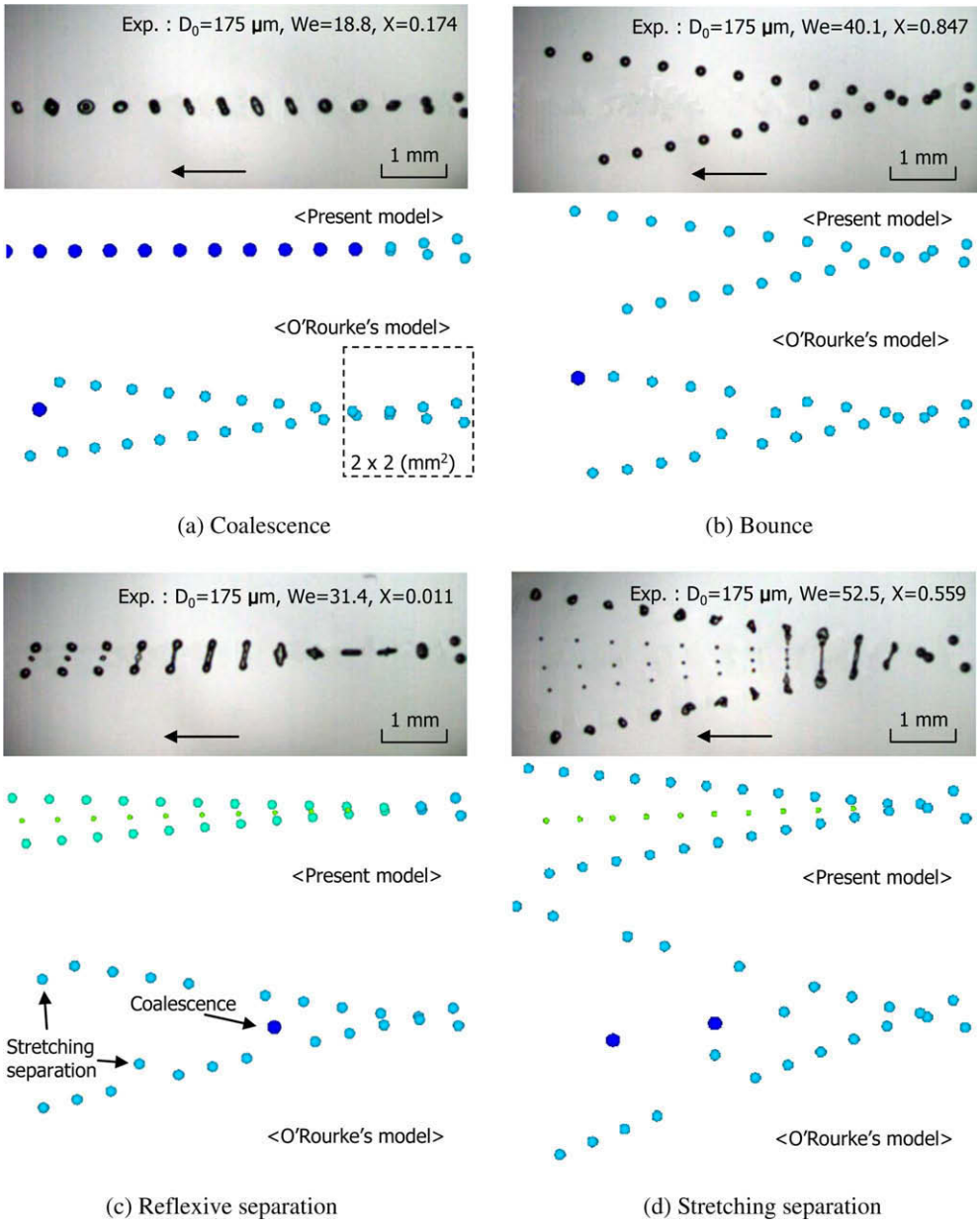

Fig. 10. Test for binary droplet collisions.

respectively. In this test, two parcel streams are injected towards a impact point having a collision angle of 45°. The number of injected parcels of the respective streams was 50, and injection velocity was 10 m/s. From the test results, the grid-independency of the present model is perfectively proved as can be seen in Fig. 12(a). The reason is that Nordin's concept is absolutely based only on the droplet's position and velocity not on the cell spacing conditions. However, the O'Rourke's model seems to have dependencies on the cell size and the grid positions from the inspections on Fig. 12(b), because the model assumes that the collision occurs only if two parcels exist in a same cell, and the collision probability is affected by the cell volume according to Eq. (5). Thus, the collision probability is heavily dependent on the position where the collision event occurs. Fig. 13 shows the calculated number of collision events of the O'Rourke's model during the whole computational time according to the impact point. By the assumption of the test, the probable number of collision events must be 50. The test proves that the parcel's position strongly influences on the collision probability, because the possibility that two parcels would be located in a same cell must be varied by the impact point. Particularly in case of the impact point ③, the collision does not occur at all, because if the impact point lies on the vertex, two parcels must exit in two different cells each other, resulting in no collision. On the other side, it can be found that the large grid resolution reduces the collision probability from the comparison between two different mesh sizes, $2 \times 2 \times 2$ mm^3 and $4 \times 4 \times 4$ mm^3.

4.3. Application to inter-impingement sprays

4.3.1. Behavior of inter-impingement sprays

Fig. 14 presents the 90° inter-impingement spray shape at $S_z = 33$ mm, when the time after the start of the injection is 2.0 ms. In this figure, the photographs was taken from the result of Chiba et al. (2000), because Maruyama et al. (2001) did not show the photograph for $S_z = 33$ mm and Chiba et al. (2000) conducted the experiments and showed the photograph under the same test conditions. Under this condition, the two sprays impacted near the breakup length, because the breakup length was 36 mm under the test conditions. Fig. 15 also shows the overall shapes of the 90° inter-impingement sprays at $S_z = 50$ mm, taken by the experiment (see Maruyama et al., 2001) and numerical simulation according to the time elapsed after injection. This case can be thought of as a spray-to-spray impingement, because the spray is fully atomized beyond the breakup length.

Contrary to the case of a binary droplet collision, the spray shape of O'Rourke's model is sufficiently impinged because there are numerous parcels in a computational cell, which makes the probability of a random collision much higher. However, in the binary droplet case, there are only two parcels in a computational cell and the collision probability is restricted to the two parcels. Therefore, in a comparison between the predicted spray shapes from the two models, the spray shape patterns are not significantly

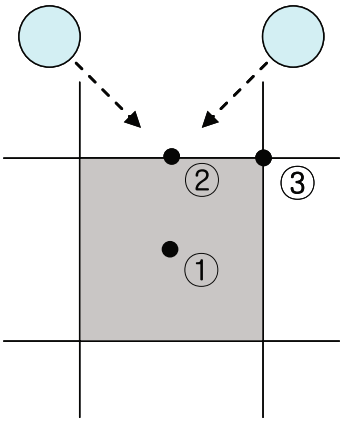

Fig. 11. Definition of the impact point (IP).

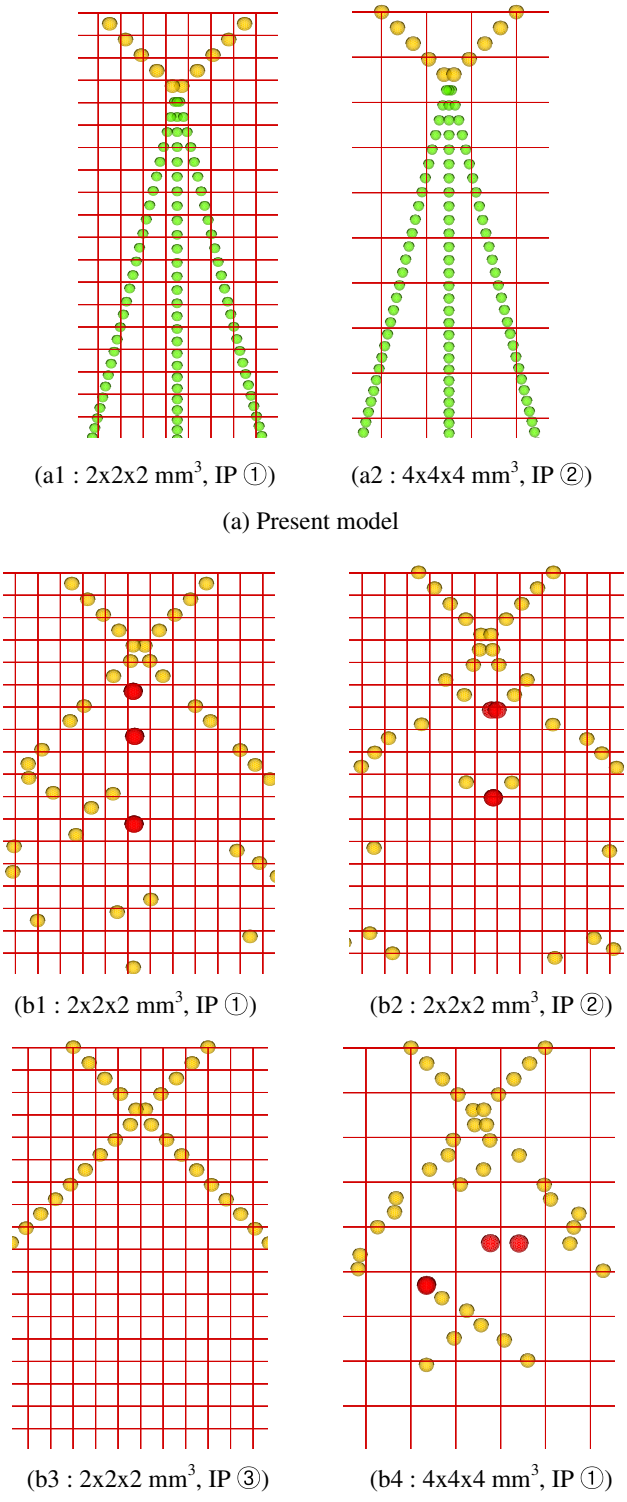

Fig. 12. Effect of grid resolution on the collision prediction.

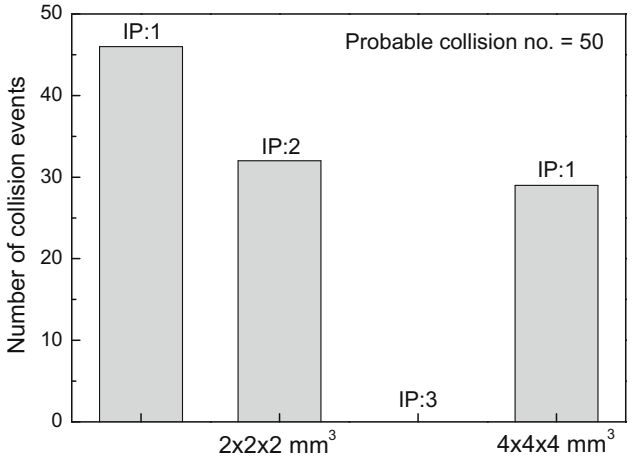

Fig. 13. Effect of grid resolution and the impact point position on the calculated number of collision events.

different. However, if the computational cell size becomes bigger than under the current condition: $2 \times 2 \times 2$ mm^3, the spray shape predicted by O'Rourke's model will change because the collision probability is determined in basis of the cell size.

On the other hand, in the case of the present model, more parcels appear inside the spray than in the case of O'Rourke's model because the present model can predict the formation of satellite droplets, which are represented by the newly added stochastic parcel, but O'Rourke's model does not generate new parcels.

4.3.2. Spray tip penetration

Fig. 16 illustrates the spray tip penetration of the non-impinged free spray and the inter-impingement sprays calculated by the present collision model and the WAVE-RT model. Since the spray tip penetration is penetrating the distance of the spray tip, the impinged spray tip penetration and the free spray tip penetration are identical to each other up to the impingement point. As shown in Fig. 16, beyond the impingement point, the tip penetration of the inter-impingement spray becomes shorter than that of the free spray, so it can be concluded that the impact of the two sprays causes a reduction in particle momentum, resulting in less of a penetrating distance. For this reason, the impingement spray at $S_z = 33$ mm has less spray tip penetration than at $S_z = 50$ mm, due to early impingement. Based on experimental observation, it has been shown that the calculated spray tip penetration correlates well with the measured spray tip penetration.

4.3.3. SMD distribution of inter-impingement spray

Fig. 17 depicts the Sauter Mean Diameter (SMD) distributions at intervals of 5 mm along the penetrating distance. Here, the penetrating distance is defined in the same way as the spray tip penetration. The experiments were conducted by Maruyama et al. (2001) and they measured the SMD at about 2 mm inside from the spray tip, where the spray has a relatively low concentration at an elapsed time of 2.0 ms after injection. As shown in Fig. 17(a), the SMD value is predicted to decrease rapidly beyond the impingement point. This pattern proves that the mutual impact of the two sprays induces frequent droplet dispersions near the impingement point. And, as already described in the case of a binary droplet collision, since the satellite droplets are always positioned between the two parent droplets, the SMD value along the penetration axis is expected to be much lower. In contrast, there is a tendency for some large droplets to be positioned radially outward. After penetrating about 10 mm beyond the impingement point, the value finally converges on a certain value. Accordingly, the assumption is that the occurrence frequency of a collision will be lower after the convergence of the SMD value.

Up to the impingement point, it is free spray such that the SMD values of the two cases must be identical regardless of nozzle position. However, there are some difference between the two cases, $S_z = 33$ mm and $S_z = 50$ mm, which are caused by the accelerated gas flow induced by the momentum transfer between the liquid and gas phases. That is, when the spray penetrates the gas phase, the gas flow is more accelerated by the gain in momentum from the liquid droplets. In particular, as the two spray axes approach each other, the surrounding gas flow is more affected by the two sprays and the accelerated gas flow stirs up the droplets. Then the droplets collide more frequently with each other, reducing the SMD value. On the other hand, the difference is not remarkable in the case of O'Rourke's model as shown in Fig. 17(b), because, in spite of the accelerated gas flow, the probability of collision is only statistically determined and the gas flow change does not noticeably affect the collision.

In the comparison between the experiment (see Maruyama et al., 2001) and currently calculated values, the present model is able to give pretty agreeable SMD values within the measurement error range, as shown in Fig. 17(a). However the O'Rourke's collision model tends to overestimate the SMD value relative to the measured value. This is due to the fact that O'Rourke's model considers only two collision outcomes, stretching separation and coalescence, and then it overestimates coalesced droplets, resulting in an increase in the SMD value. But, the SMD value predicted by O'Rourke's model begins to increase even before the impingement point, while the value from the present model converges on a certain value near the impingement point. This suggests that the

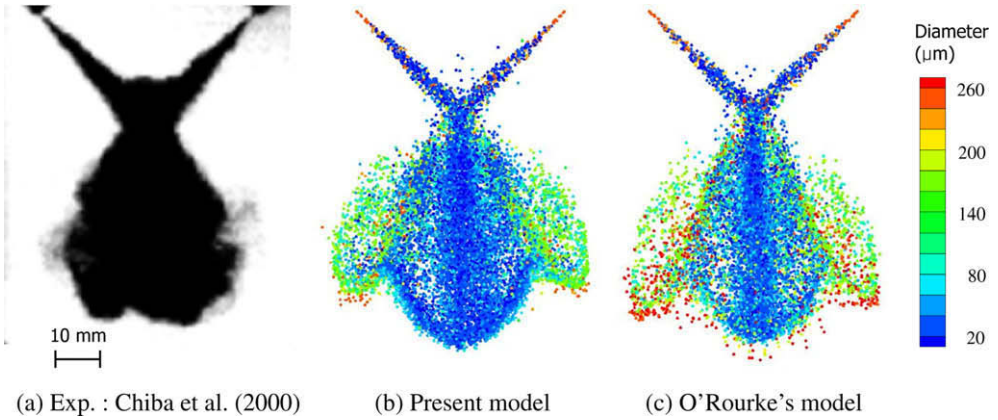

Fig. 14. Inter-impingement spray shape at $S_z = 33$ mm and $t_{inj} = 2.0$ ms.

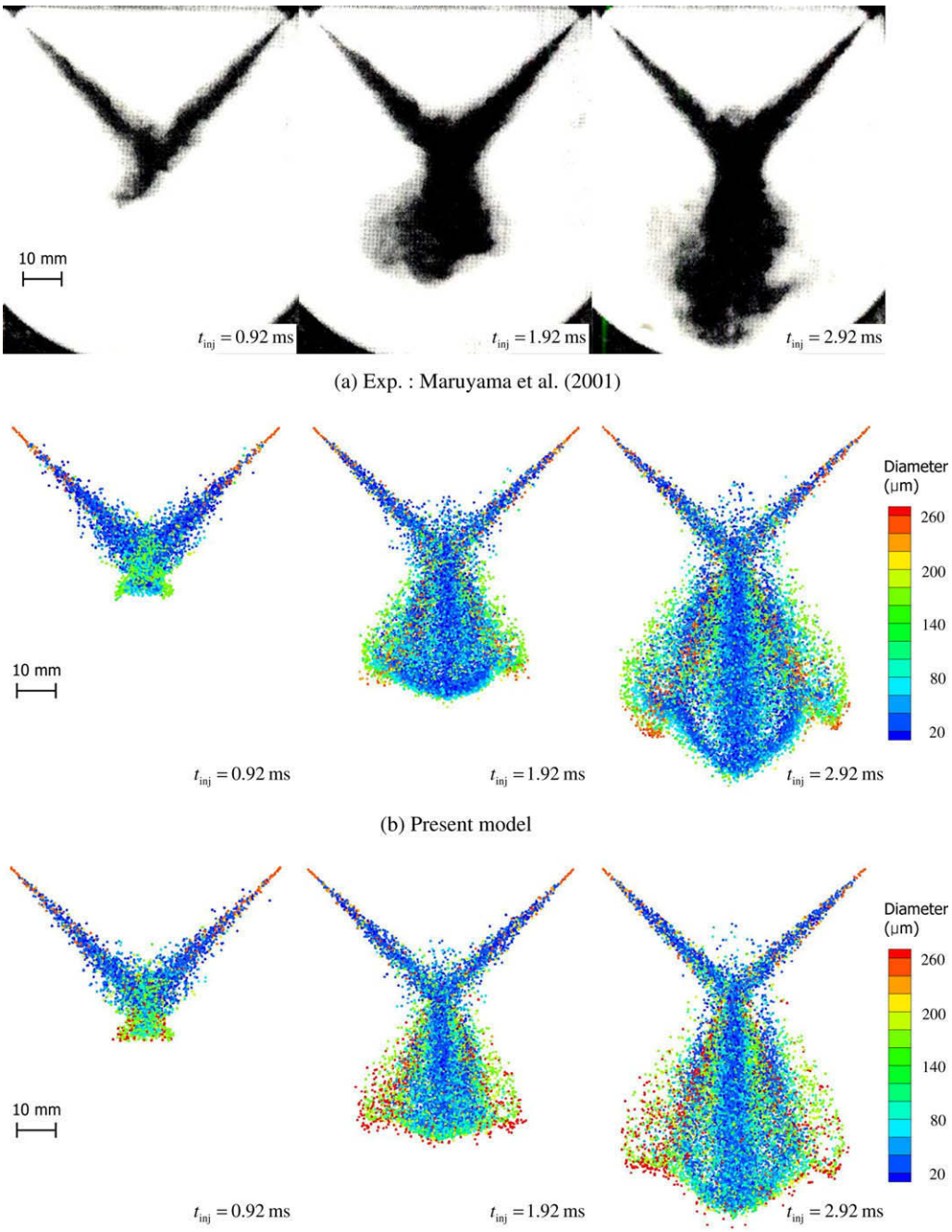

Fig. 15. Inter-impingement spray shape at S_z = 50 mm according to the injection time.

collisions are predicted to occur frequently when the spray is moderately atomized, even before the impingement.

Fig. 18 shows the SMD distributions in the radial direction. In the figure, the DFIP is an abbreviation for Distance from Impingement Point, which measures from the impingement point downward. As previously discussed, the SMD values along the penetration axis are much lower than those distributed radially outward, and this pattern is observed in Fig. 18. As soon as the two sprays impact, the SMD distribution pattern shows a V-type. And as the spray penetrates, the somewhat large droplets tend to be spread out radially. In contrast, O'Rourke's model results in larger SMD values than the present model because O'Rourke's model tends to show an overestimation of coalescence collisions.

4.3.4. Droplet velocity distribution of inter-impingement spray

The effect of the accelerated gas on the droplet behavior can be verified by inspecting the droplet mean velocity distribution. Fig. 19 demonstrates the droplet mean velocity distributions along the spray penetrating distance and up to a penetrating distance of 33 mm, the droplet mean velocities of S_z = 33 mm are higher than those of S_z = 50 mm. That is to say, since the two spray axes are in close proximity, particularly in the case of S_z = 33 mm, the droplets are apt to be stirred and accelerated due to the downward accelerated gas flow. In the meantime, after the two sprays impact, the mean droplet velocity rapidly decreases owing to the momentum loss induced by the droplet interactions. After the brief and rapid decrease in velocity, the velocity starts to decrease with a constant

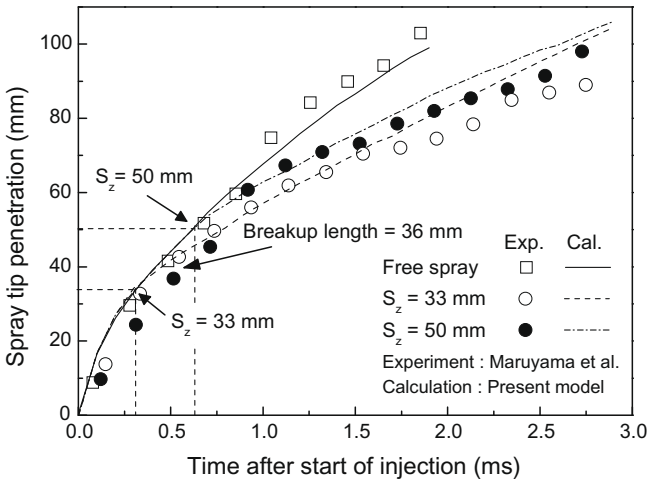

Fig. 16. Spray tip penetration.

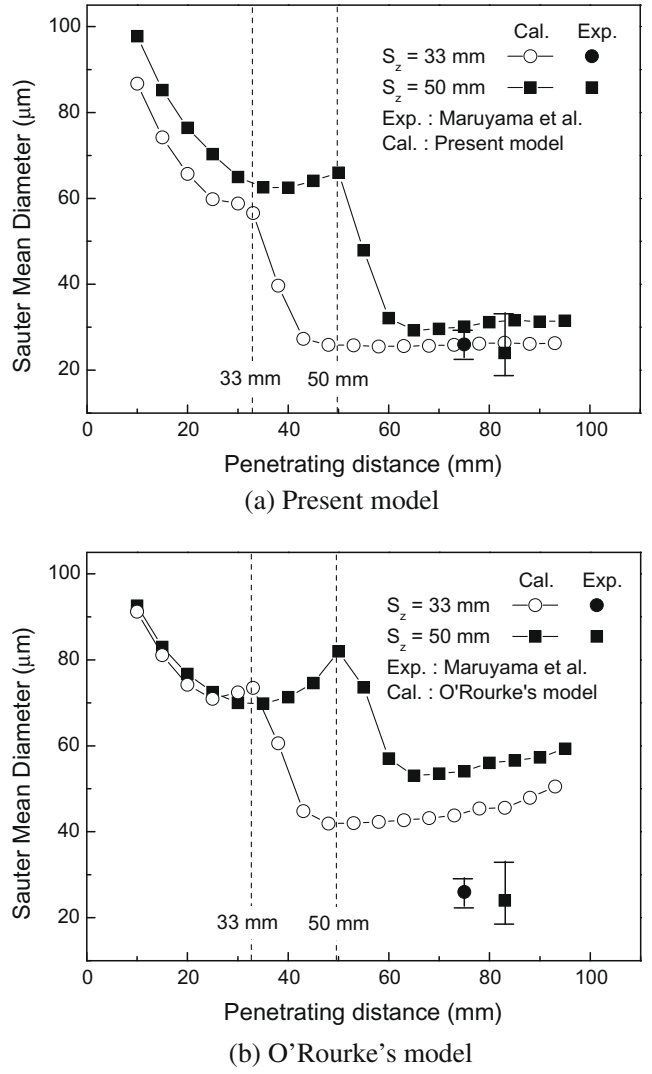

Fig. 17. SMD distribution along the penetrating distance.

deceleration. Therefore, the majority of total collisions occur in the short period of rapidly decelerating velocity.

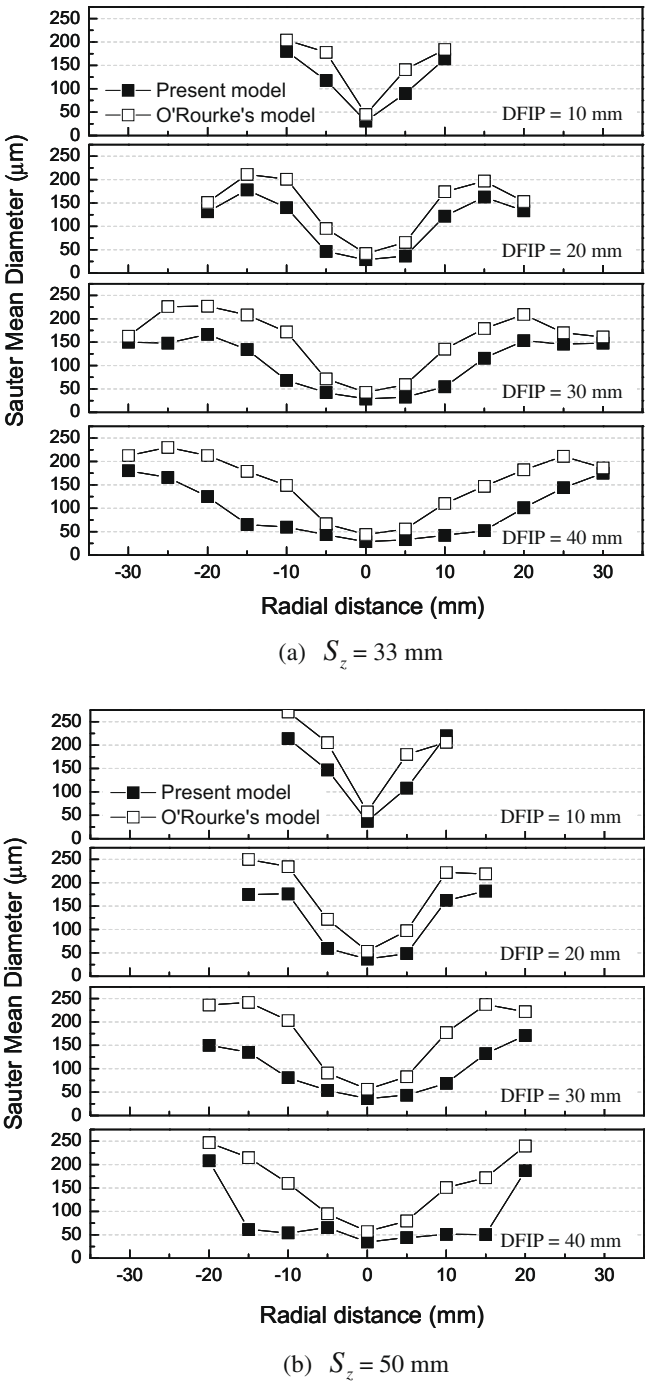

Fig. 18. SMD distribution in the radial direction.

4.3.5. Overall SMD

Fig. 20 shows the calculated overall SMD in terms of elapsed time. The overall SMD was calculated by averaging the entire droplet diameter. In this figure, the O'Rourke's model gives an apparently higher SMD value than the present model because the O'Rourke's model considers only two main outcomes, one of which is coalescence. In the results from the present model, after the impingement, the overall SMD begins to increase slightly, and then converges on a certain value. But the calculated overall SMD by O'Rourke's model suddenly increases at the same point, even before the impingement. This pattern can also be observed in the SMD distribution shown in Fig. 17(b). In addition, in the comparison between the two injection cases i.e., $S_z = 33$ mm and

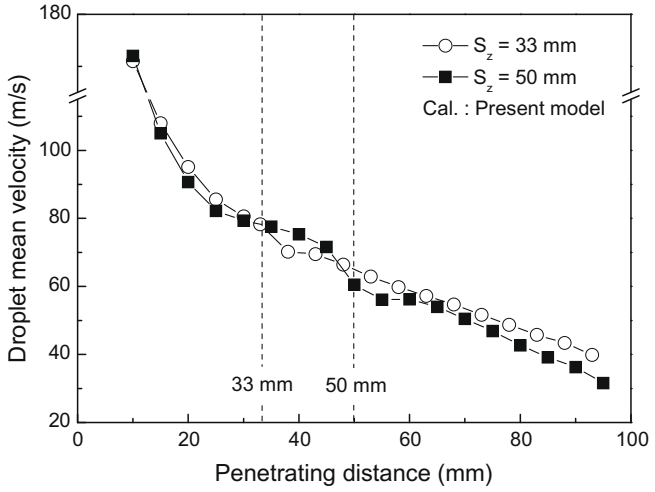

Fig. 19. Droplet mean velocity distribution.

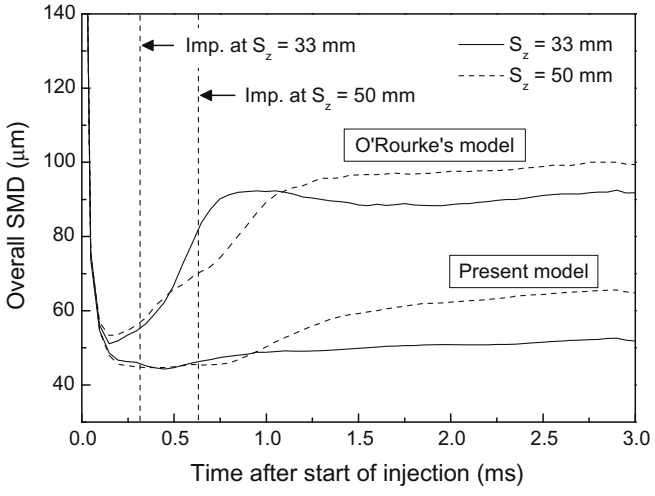

Fig. 20. Calculated overall SMD.

S_z = 50 mm, the overall SMD value of S_z = 33 mm is expected to be higher than that of S_z = 50 mm. This expectation is due to the fact that the longer the impingement distance is, the lower the droplet velocity near the impingement point, as demonstrated by Fig. 19. As a result, coalescence is more likely to happen due to the low colliding velocity.

4.3.6. Collision outcome ratio

Fig. 21 illustrates the cumulative collision outcome ratio calculated by the two models in terms of elapsed time. Here, the collision ratio is defined as the number of the targeted collision outcomes over the total number of collisions, which represents how frequently individual collision outcomes occur during the entire spraying process. Using the present model calculation, we can find all the possible collision outcomes and the probability of each outcome includes a series of stretching separation, coalescence, bounce and reflexive separation. By analyzing the collision ratio, we expect that the collision process is governed by the competition between stretching separation and coalescence outcomes. However, in the case of the O'Rourke's model, nothing but the coalescence and the stretching separation are predicted owing to its assumption on the collision outcome. In addition, the probability of coalescence occurrence is predicted to be twice that of the probability of stretching separation. As a result, the SMD values are impractically high, as demonstrated in Figs. 17, 18 and 20. Furthermore, O'Rourke's model tends to predict collisions as soon as the spray injects because the model assumes that two parcels collide only if they lie in the same computational cell.

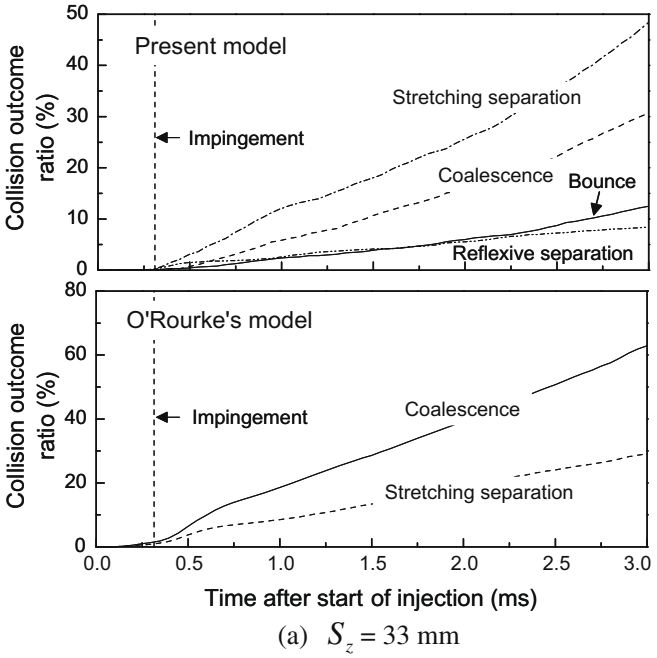

(a) $S_z = 33$ mm

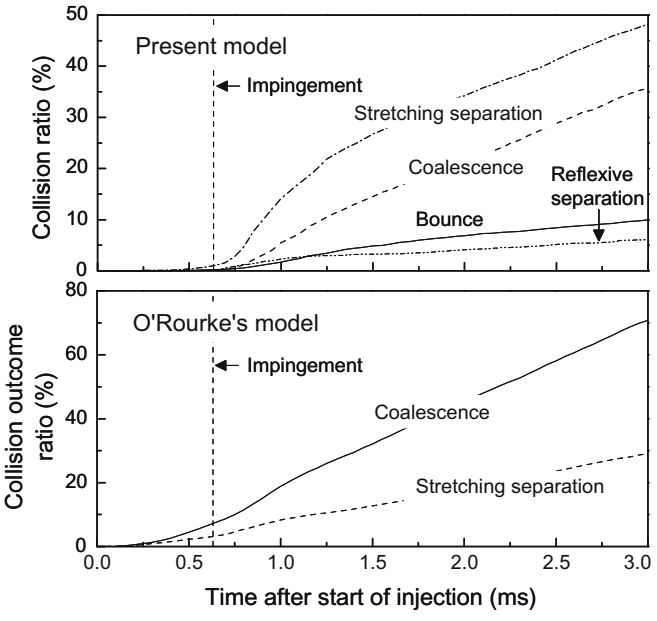

(b) $S_z = 50$ mm

Fig. 21. Cumulative collision outcome ratio (%).

4.4. Effect of total parcel number on the calculated results

In order to investigate the effect of total parcel number on the calculated SMD results, the test was conducted for various parcel number as 3000, 4000, and 5000 and test condition of S_z = 50 mm. Fig. 22(a) shows the SMD distribution along the penetrating distance according to type of the collision models. In case of the present model, the calculated SMD result seems to be influenced by variation of the total parcel number, that is, the more parcels are applied, the higher SMD value becomes. Especially, the effect of

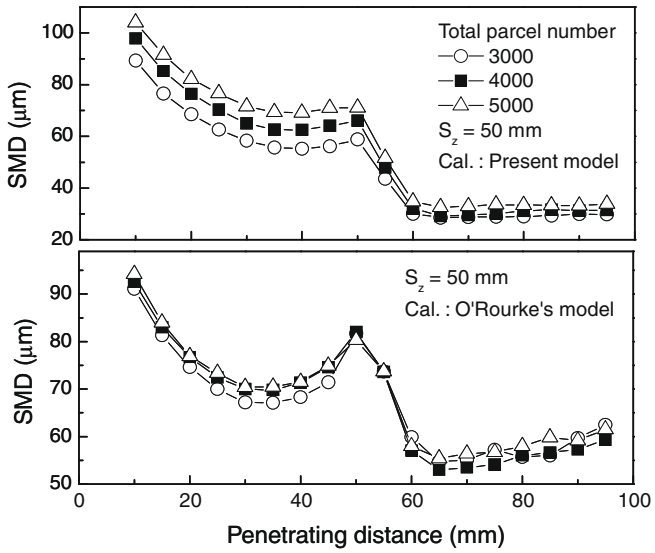

(a) SMD distribution along the penetrating distance

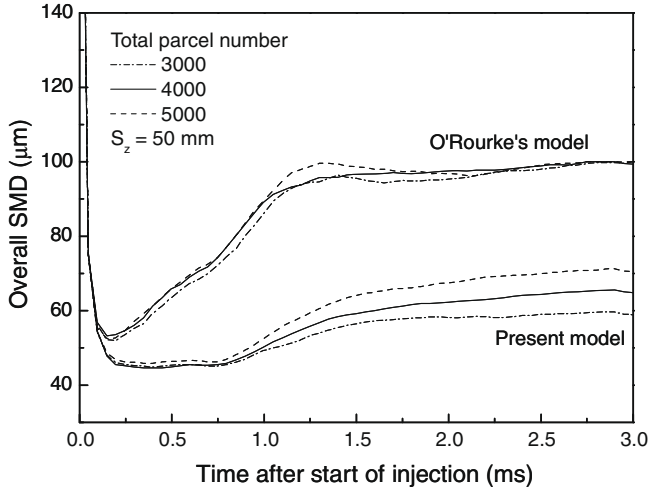

(b) Overall SMD

Fig. 22. Influence of the total parcel number on the calculated results.

parcel number variation on the SMD result gets remarkable up to the impingement point, where the free spray region is. This indicates that the total parcel number slightly influences the collision probability of the present model because Nordin's concept considers only parcel-to-parcel geometrical relation. This pattern also appears in the result of overall SMD as shown in Fig. 22(b). On the other hand, results of the O'Rourke's model seem to be rarely affected by the variation of the parcel number owing to its assumption on the collision probability. From the test result, parcel number independent collision algorithm needs to be developed to obtain more accurate predictions.

5. Conclusions

In the present work, simulations of binary droplet collision and inter-impingement sprays were conducted using two kinds of collision models, with one based on a statistical approach and the other on a deterministic approach. In order to accurately predict droplet collisions, we used the present collision modeling method with a deterministic approach for collision conditions and the post-collision characteristics, and the Munnannur's fragmenting collision model with a consideration for all collision outcomes. Then, we attempted to validate and compare O'Rourke's collision model and our suggested droplet collision model by comparing the experimental results with the model calculations. Our study provided the following results:

1. The practical collision outcomes can be subdivided according to Weber number-Impact parameter curves derived from preceding studies (see e.g. Ashgriz and Poo, 1990; Brazier-Smith et al., 1972; Estrade et al., 1999). Therefore it is appropriate to implement the criteria for droplet collision regimes into the CFD code in consideration of all possible collision outcomes. In addition, the distribution satellite droplet numbers on the Weber number-Impact parameter domain can be predicted when using the modified criteria from Munnannur's collision model.

2. In the case of O'Rourke's collision model, the collision condition is determined statistically so that a collision would not occur even if the two parcels are placed in close proximity. On the other hand, by applying a deterministic approach in collision modeling, the probability of the collision can be practically calculated. And Munnannur's fragmenting collision model makes it possible to predict the formation of satellite droplets in cases of stretching separation and reflexive separation, and gives a good prediction of the number of satellite droplets when modifying the model's criteria assumption.

3. In the comparison of mean droplet size, while O'Rourke's model tends to overestimate SMD, the present model can provide reasonable values for SMD because it is able to simulate the formation of satellite droplets due to the application of Munnannur's fragmenting model. In particular, since the collision probability of the present model is determined by actual droplet movement, the model can demonstrate the effect of the accelerated gas flow induced by momentum transfer between the spray and gas phase. Thus, the gas flow effect does affect the collision probability, and the results with the present model are in good agreement with the experimental SMD results.

4. The present model involves all possible collision outcomes and therefore can prevent any abnormal increases in SMD according to the injection time. Particularly, the overall SMD begins to increase after the impingement point in the present model with deterministic modeling of the collision probability, whereas the statistical approach for assessing collision probability utilizes the active collision process within the free spray region, which results in a sudden increase in the overall SMD before the impingement point.

5. Based on the collision outcome ratio resulting from the present model, stretching separation and coalescence represent a large portion of total collision outcomes. Therefore, we can conclude that the collision process is dominated mainly by the competition between stretching separation and coalescence outcomes.

Acknowledgements

This study was supported by the CEFV (Center for Environmentally Friendly Vehicle) of the Eco-STAR project from MOE (Ministry of Environment, Republic of Korea). This work was also supported by the Korea Research Foundation Grant funded by the Korean Government (MOEHRD, Basic Research Promotion Fund) (KRF-2006-511-D00081).

Appendix A

A.1. Determination of droplet velocity after collision: separation regimes

When two droplets travel toward each other in three-dimensional space, the momentum change naturally occurs in the

direction of the relative velocity vector. Therefore, the vector components of the velocity of a moving droplet must be decomposed into a portion along the relative velocity direction and the respective normal direction. Then the equation for velocity change should be applied only to the relative velocity vector component. Fig. A1 shows the schematic for colliding droplets at the moment of contact and the dotted lines indicate the directions of relative vector (*rel.*) and its normal vector (*nrel.*). The relative velocity vector is determined by

$$\vec{u}_{12} = \vec{u}_2 - \vec{u}_1 \tag{A1}$$

The magnitude of the velocity components codirectional to the relative velocity is represented as scalar projection of the droplet velocity onto the relative velocity and can be derived by

$$|\vec{u}_{i,rel}| = \vec{u}_i \cdot \hat{u}_{12} \quad (i = 1,2), \tag{A2}$$

where $\hat{u}_{12}$ is the unit vector codirectional to $\vec{u}_{12}$. When the scalar quantity $|\vec{u}_{i,rel}|$ is multiplied by the vector $\hat{u}_{12}$, a vector form of droplet velocity along $\vec{u}_{12}$ can be obtained. In addition, as $\vec{u}_{i,rel}$ is given, the normal component of the droplet velocity to $\vec{u}_{12}$ can also be resolved:

$$\vec{u}_{i,rel} = |\vec{u}_{i,rel}|\hat{u}_{12} \quad (i = 1,2) \tag{A3}$$

$$\vec{u}_{i,nrel} = \vec{u}_i - \vec{u}_{i,rel} \quad (i = 1,2) \tag{A4}$$

However, it is important to note that, by decomposing the vectors on the right side of Eq. (A1) into *rel.* and *nrel.*, Eq. (A1) can be rearranged as

$$\vec{u}_{12} = \vec{u}_{2,rel} + \vec{u}_{2,nrel} - \vec{u}_{1,rel} - \vec{u}_{1,nrel} \tag{A5}$$

Here, since $\vec{u}_{12}$ coincides with the *rel.* direction, $\vec{u}_{2,nrel} - \vec{u}_{1,nrel}$ must be zero such that $\vec{u}_{2,nrel}$ is equal to $\vec{u}_{1,nrel}$.

Because the momentum change must happen in the *rel.* direction, Eq (8) should be applied only to $\vec{u}_{i,rel}$. Denoting the changed velocity by $\vec{u}'_{i,rel}$, the corrected velocity of the interacting droplet can be calculated as

$$\vec{u}'_i = \vec{u}'_{i,rel} + \vec{u}_{i,nrel} \quad (i = 1,2) \tag{A6}$$

In Eq. (8), z represents the fraction of dissipated energy during the collision. According to the suggestion by Brazier-Smith et al. (1972), Eq. (8) should be used for stretching separation. But reflexive separation, z, is determined by

$$z = \sqrt{1 - \frac{We_{rflx}}{We}} \tag{A7}$$

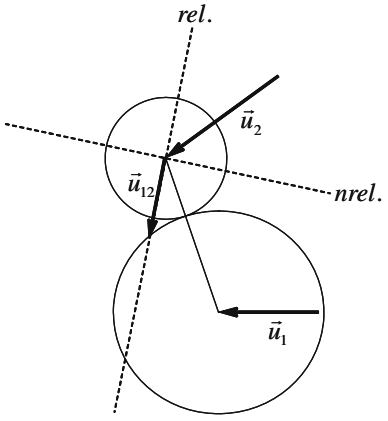

Fig. A1. Schematic of colliding droplets: vector decomposition based on the relative velocity.

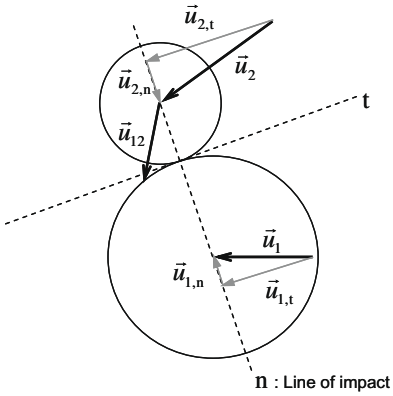

Fig. A2. Schematic of colliding droplets: vector decomposition based on the contact surface.

where We_{rflx} is the critical Weber number for the reflexive separation as calculated by Eq. (25).

In the current study, when a satellite droplet is formed from the ligament, the satellite droplet is assumed to move toward the *nrel.* direction with a velocity that has the magnitude of $|\vec{u}_{i,nrel}|$. Here, it does not matter if i is 1 or 2, because $\vec{u}_{1,nrel} = \vec{u}_{2,nrel}$ as already discussed. So the velocity of satellite droplet becomes

$$\vec{u}_{sat} = \vec{u}_{1,nrel} \tag{A8}$$

A.2. Determination of droplet velocity after collision: Bouncing regimes

A droplet bouncing can be considered as an oblique central impact between two rigid spheres. Let us now consider the case when the two spheres impact along an oblique line to the contact surface as depicted in Fig. A2. The n axis along the line of impact, and the t axis along the common tangent can be chosen. Since the only impulses are always exerted on the spheres due to internal forces directed along the line of impact, the vector components of their velocities must be decomposed into a portion along the line of impact and the tangential line.

Assuming the two droplet positions are $\vec{p}_1 = (x_1, y_1, z_1)$ and $\vec{p}_2 = (x_2, y_2, z_2)$, respectively, the distance vector between the two droplets is $\vec{D}_{12} = \vec{p}_2 - \vec{p}_1$, the magnitude of velocity component along the line of impact and the tangential line, $\vec{u}_{i,n}$, and $\vec{u}_{i,t}$ is derived in the same way as Eq. (A2), (A3). Then, the value of $\vec{u}_{i,t}$ should not change because the impact happens only along the n axis. Next, the magnitude of the changed velocity along the n axis, $|\vec{u}'_{i,n}|$ can be derived by conservation of momentum and by defining the coefficient of restitution, e as:

$$\vec{u}'_{i,n}| = \frac{1}{m_i + m_j}\{m_i|\vec{u}_{i,n}| + m_j|\vec{u}_{j,n}| - e(\vec{u}_{i,n}| - |\vec{u}_{j,n}|)m_j\} \quad (i,j = 1,2) \tag{A9}$$

Here, the coefficient of restitution e is set to unity, because the droplet bouncing is assumed to be same as a perfectly elastic impact. This means that the relative velocities before and after collision are equal. After collision, the velocity vector along the n axis is determined by multiplying the quantity derived in Eq. (A9) by the unit vector of $\vec{u}_{i,n}$. Then the final velocity vector of the each droplet is determined as the sum of the changed velocity vector and tangential vector as:

$$\vec{u}'_i = \vec{u}'_{i,n} + \vec{u}'_{i,t} \quad (i = 1,2) \tag{A10}$$

References

Amsden, A.A., 1997. KIVA-3V: a block structured KIVA program for engines with vertical or canted valves, Technical report, No. LA-13313-MS. Los Alamos National Laboratory.

Ashgriz, N., Poo, J.Y., 1990. Coalescence and separation in binary collisions of liquid drops. J. Fluid Mech. 221, 183–204.

Aumann, R., McCracken, M., and Abraham, J., 2002. An evaluation of a composite model for predicting drop–drop collision outcomes in multidimensional spray computations. SAE paper 2002-01-0943.

Beale, J.C., Reitz, R.D., 1999. Modeling spray atomization with the Kelvin–Helmholtz/Rayleigh–Taylor hybrid model. Atomization Sprays 9, 623–650.

Blei, S., Ho, C.A., Sommerfeld, M., 2002. A stochastic droplet collision model with consideration of impact efficiency, CD-ROM of Proc. ILASS-Europe 2002.

Brazier-Smith, P.R., Jennings, S.G., Latham, J., 1972. The interaction of falling rain drops: coalescence. Proc. R. Soc. London, Ser. A 326, 393–408.

Brenn, G., Valkovska, D., Danov, K.D., 2001. The formation of satellite droplets by unstable binary drop collisions. Phys. Fluids 13 (9), 2463–2477.

Chen, R.-H., 2007. Diesel-diesel and diesel-ethanol drop collisions. Appl. Thermal Eng. 27, 604–610.

Chiba, T., Saito, M, Amagai, K., and Arai, M., 2000. Inter-spray impingement of two diesel sprays, CD-ROM of Proc. 8th ICLASS.

Dukowicz, J.K., 1980. A particle-fluid numerical model for liquid sprays. J. Comput. Phys. 35, 229–253.

Estrade, J.-P., Carentz, H., Lavergne, G., Biscos, Y., 1999. Experimental investigation of dynamic binary collision of ethanol droplets-a model for droplet coalescence and bouncing. Int. J. Heat Fluid Flow 20, 486–491.

Georjon, T.L., Reitz, R.D., 1999. A drop-shattering collision model for multidimensional spray computations. Atomization Sprays 9, 231–254.

Ko, G.H., Lee, S.H., Ryou, H.S., Choi, Y.K., 2003. Development and assessment of a hybrid droplet collision model for two impinging sprays. Atomization Sprays 13, 251–272.

Ko, G.H., Ryou, H.S., 2005. Droplet collision processes in an inter-spray impingement system. J. Aerosol Sci. 36, 1300–1321.

Maruyama, Y., Chiba, T., Saito, M., Arai, M., 2001. Effect of the inter-impingement process on the behavior of a diesel spray. In: Proc. ILASS-Asia 2001, pp. 241–246.

Munnannur, A., Reitz, R.D., 2007. A new predictive model for fragmenting and non-fragmenting binary droplet collisions. Int. J. Multiphase Flow 33, 873–896.

Nordin, N., 2000. A mesh independent collision condition for Lagrangian sprays. Thermo and Fluid Dynamics. Chalmers University of Technology.

Orme, M., 1997. Experiments on droplet collisions, bounce, coalescence and disruption. Energy Combust. Sci. 23, 65–79.

O'Rourke, P.J., 1981. Collective drop effects on vaporizing liquid sprays, Ph.D. thesis, Mechanical and Aerospace Engineering, Princeton University, USA.

O'Rourke, P.J., Bracco, F.V., 1980. Modeling of drop interactions in thick sprays and a comparison with experiments. Proc. IMech. E. 9, 101–116.

Park, S.W., Kim, H.J., Lee, C.S., 2003. Investigation of atomization characteristics and prediction accuracy of hybrid models for high-speed diesel fuel sprays. SAE Paper 2003-01-1045.

Qian, J., Law, C.K., 1997. Regimes of coalescence and separation in droplet collision. J. Fluid Mech. 331, 59–80.

Rayleigh, L., 1878. On the instability of jets. Proc. London Math. Soc. 110:4.

Reitz, R.D., 1987. Modeling atomization processes in high-pressure vaporizing sprays. Atomization Sprays 3, 309–337.

Reitz, R.D., Diwakar, R., 1987. Structure of high-pressure fuel sprays. SAE paper 870598.

Sommerfeld, M., 2001. Validation of a stochastic Lagrangian modelling approach for inter-particle collisions in homogeneous isotropic turbulence. Int. J. Multiphase Flow 27, 1829–1858.

Su, T.F., Patterson, M.A., Reitz, R.D., Farrell, P.V., 1996. Experimental and numerical studies of high pressure multiple injection sprays. SAE paper 960861.